J Mater Sci: Mater Electron (2008) 19:305–309
DOI 10.1007/s10854-007-9339-9

Raman scattering studies of ultrashallow Sb implants in strained Si

L. O'Reilly · N. S. Bennett · P. J. McNally · B. J. Sealy · N. E. B. Cowern · A. Lankinen · T. O. Tuomi

Published online: 21 June 2007

Abstract Sheet resistance (R_s) reductions are presented for antimony doped layers in strained Si. We use micro-Raman spectroscopy to characterise the impact of a low energy (2 keV) Sb implantation into a thin strained Si layer on the crystalline quality and resultant stress in the strained Si. The use of 325 nm UV laser light enables us to extract information from the top ~9 nm of the strained Si layer. Prior to implantation the Si layer is fully strained with a tensile stress value ~1.41 GPa, in agreement with the calculated theoretical maximum on a strain relaxed buffer with 17% Ge content. There is a clear decrease in the intensity of the Si Raman signal following Sb implantation. The lattice damage and lattice recovery achieved by subsequent rapid thermal anneal (RTA) is quantified using the amplitude and full width at half maximum (FWHM) of the crystalline Si peak. The shift of the Raman Si peak is a key parameter in the interpretation of the spectra. The ion-implanted sample is studied in terms of a phonon coherence length confinement model. Carrier concentration effects are seen to play a role in the Raman shift following electrical activation of the Sb atoms by RTA.

L. O'Reilly (✉) · P. J. McNally
Nanomaterials Processing Laboratory,
Research Institute for Networks and Communications Engineering (RINCE), School of Electronic Engineering,
Dublin City University, Glasnevin, Dublin 9, Ireland
e-mail: oreillyl@eeng.dcu.ie

N. S. Bennett · B. J. Sealy · N. E. B. Cowern
Advanced Technology Institute, University of Surrey, Guildford GU2 7XH, UK

A. Lankinen · T. O. Tuomi
Micro and Nanosciences, Micronova, Helsinki University of Technology, P.O. Box 3500, Espoo 02015 TKK, Finland

1 Introduction

The ability to improve performance consistently while decreasing power consumption has made CMOS architecture the dominant technology for integrated circuits. The scaling of the CMOS transistor has been the primary factor driving improvements in microprocessor performance [1]. Strain engineering using Si/SiGe heterostructures is a key technology for the enhancement of device operating speeds. The production of ultrashallow junctions for the source/drain extension region using low energy ion-implantation will be required for future CMOS devices. The extent to which strain engineering can be successfully combined with ion-implantation doping of ultrashallow source-drain regions will depend on the effects of strain on dopant diffusion and activation at high dopant concentrations. Arsenic is the standard n-type dopant species in Si. We investigate Sb as a possible alternative to As, due to improvements in junction depth and abruptness resulting from its greater mass.

2 Experimental details

Experiments were performed on IQE tensile strained Si wafers grown on constant-composition $Si_{0.83}Ge_{0.17}$ relaxed buffer layers. Each wafer was implanted with a low energy (2 keV) Sb implant to a dose of 4×10^{14} cm^{-2} creating a junction at 12 nm, as defined by dopant concentration fall-off to the 3×10^{18} cm^{-3} level. Control samples were prepared using conventional p-type Si wafers for comparison. The quality of the SiGe substrates was investigated using white beam synchrotron X-ray topography. The synchrotron X-ray topography measurements were performed at HASYLAB-DESY and ANKA. The Hamburger Synchrotronstrahlungslabor am Deutschen Elektronen-Synchrotron

(HASYLAB-DESY) utilises the continuous spectrum of synchrotron radiation from the DORIS storage ring bending magnet. The ring operates at positron energies of 4.45 GeV and at typical currents of 80–150 mA. At the recently constructed Angströmquelle Karlsruhe, (ANKA, Karlsruhe, Germany) synchrotron light source, a small point source of 0.5×0.2 mm^2 at a bending magnet of the 2.5 GeV storage ring provides light with a characteristic wavelength of 2 Å and typical beam currents of 100–200 mA. The topograph patterns are recorded on high-resolution Slavich VRP-M X-ray films with a grain size of approximately 0.05 μm. Van der Pauw sheet resistance measurements were used to compare the resistivity of Sb-implanted samples in unstrained and strained Si wafers to values obtained for As in strained Si. Room temperature micro-Raman measurements were performed with a Jobin Yvon LabRam HR800 system in backscattering geometry using a 325 nm He–Cd UV laser excitation with a spot size of approximately 1 μm. Each spectrum was averaged over at least ten acquisitions to reduce noise effects.

3 Results and discussion

3.1 Synchrotron X-ray topography

An example of a large area, back-reflection topograph is shown in Fig. 1. The penetration depth (t_p) of the X-rays for this $1\bar{1}7$ reflection is 15.8 μm. Therefore the entire SiGe buffer layer is being imaged in this geometry. The projection of the diffraction vector g, onto the plane of the recording film is indicated in the figure. We see a well-defined crosshatched pattern with ridges running along two perpendicular ⟨011⟩ directions. This is characteristic of misfit dislocations. The presence of misfit dislocations verifies that there is strain relaxation in the SiGe buffer layers, as expected. We do not see any evidence of other defects in the topograph, confirming that the substrates used are of high quality.

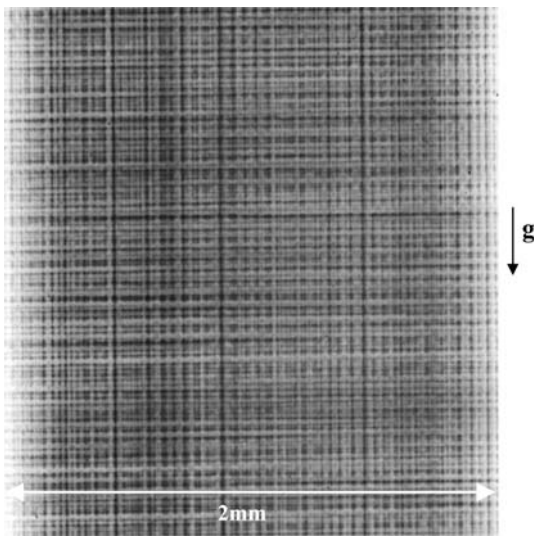

Fig. 1 Large area back reflection topograph, $1\bar{1}7$reflection, t_p = 15.8 μm

3.2 Electrical measurements

Van der Pauw sheet resistance measurements as a function of anneal temperature are shown in Fig. 2. A significant reduction in R_s is measured for Sb implants in strained Si compared to bulk unstrained material. The reduction in electrical activation, resulting in an increased R_s value of Sb in bulk Si at 800 °C, is in agreement with studies by Alzanki et al. [2]. Previous investigations of the electrical properties have indicated that this R_s lowering in strained Si, results not only from strain enhanced mobility, but also from an improvement in electrical activation of Sb with strain [3]. Earlier work examining As indicates that this Sb behaviour differs from that of As in which sheet resistance measurements of As in bulk and strained-Si layers performed by Dilliway et al. [4] showed a reduction in the R_s value in strained material resulting from a 15% higher electron mobility in the strained (20% Ge) material, but no evidence was found for a difference in electrically active As concentrations as a function of strain. This is confirmed here, by our comparison of the sheet resistance values of Sb and As in strained Si under identical implant and annealing conditions showing a clear decrease in R_s for the Sb case.

3.3 Micro-Raman spectroscopy

The Raman spectra of the strained-Si and reference Si samples (Fig. 3) are dominated by the signal of the

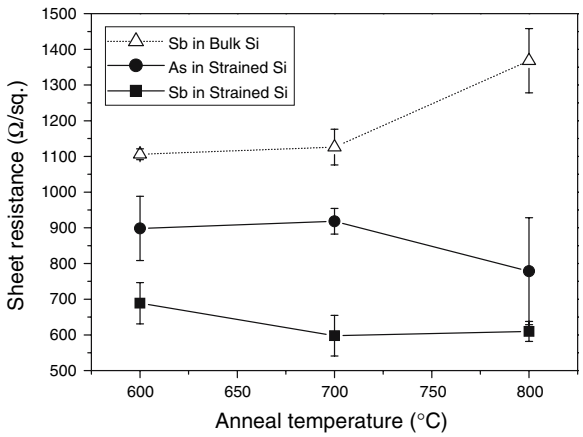

Fig. 2 R_s measurements as a function of annealing temperature for 2 keV, 4×10^{14} cm^{-2} Sb implants into bulk and strained Si, and As implants in strained Si

degenerate Si–Si Raman peak. For the bulk Si wafer, this Si peak appears at a Raman shift of ~520 cm^{-1}. A red shift (lower wavenumber) in the Si–Si Raman peak position of the strained Si samples compared to that of the reference unstrained Si sample confirms that a tensile stress is present in the Si cap layer. Using the average Si–Si phonon peak position, the biaxial stress in the Si cap layer before Sb implantation was calculated from $\Delta\omega_{Si_{UV}}$ using the equation $\sigma_{xx} = \sigma_{xy} = -\Delta\omega_{Si_{UV}}/4$ (GPa) [5], where $\Delta\omega_{Si_{UV}}$ is the Si–Si Raman peak shift compared to that of the reference Si sample obtained using the UV laser, and $\sigma_{xx} = \sigma_{yy}$ are the stress components of the biaxial stress in the x–y plane. Therefore the measured peak shift of –5.64 ± 0.1 cm^{-1} corresponds to a stress of 1.41 ± 0.03 GPa. In the case of a fully strained Si cap layer, the tensile stress σ_f in the Si cap can be calculated with the following equation [6]: $\sigma_f = Y_f m/(1 - v)$, where Y_f is the film Young's modulus, m is the misfit between the film and the substrate lattice parameters and v is Poisson's ratio of the film. By estimating the lattice constant of a fully relaxed $Si_{0.83}Ge_{0.17}$ the misfit between the Si cap and SiGe buffer layer is found to be ~0.71%. Thus the tensile stress for a fully strained Si layer on $Si_{0.83}Ge_{0.17}$ is calculated as 1.28 GPa, which is close to the experimentally measured value.

The Si Raman peak intensity before and after implantation and heat treatment for both strained Si and bulk Si samples is plotted in Fig. 4. It is noted that before ion implantation, the Si Raman peak amplitude of the strained Si sample is somewhat lower than that of the bulk Si reference and the FWHM of the strained Si peak, 3.8 cm^{-1} is slightly larger than that of the Raman peak of the bulk Si, 3.5 cm^{-1}. This suggests that the crystalline quality of the thin, 17 nm strained Si film is not quite as good as that of the bulk Si wafer. Following Sb implantation, the intensity of the Si–Si mode Raman peak decreases to approximately

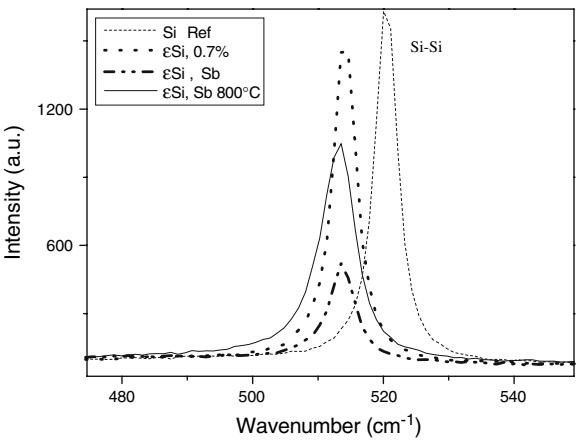

Fig. 3 UV Raman spectra of Sb-implanted and strain free Si reference sample

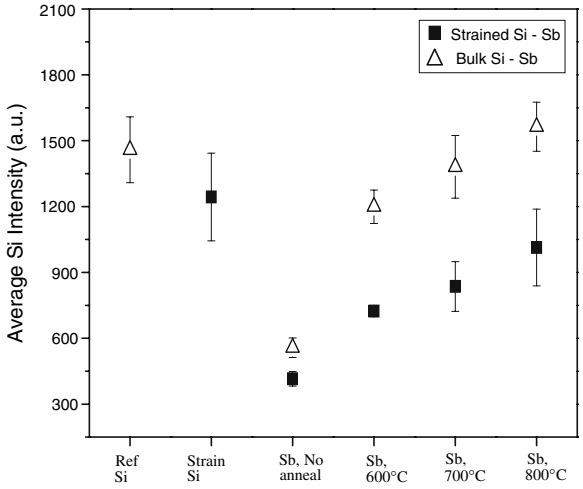

Fig. 4 Average Peak amplitude of the Si–Si Raman mode in Sb-implanted Strained and Bulk Si substrates

half of that of the strained Si sample prior to implantation and the FWHM increases from 3.8 cm^{-1} to 4.3 cm^{-1}, respectively, indicating an increase in lattice disorder. After RTA at 600 °C for 10 s, the lattice damage induced by the ion-implantation begins to be repaired, and therefore the amplitude of the Si peak increases. A further increase in intensity is detected following RTA at 700 and 800 °C. The amplitude of the Si Raman peak has recovered to its original value in the case of the bulk Si after annealing at 800 °C. However, the lattice recovery is not complete in the strained Si samples.

The Si Raman peak position was extracted using a Gauss/Lorentz fitting function for each of the strained Si and bulk Si samples. The Raman shift relative to the reference Si peak position for bulk samples and the normalised Raman shift relative to the strained Si peak position for strained Si samples are compared in Fig. 5 as a function of annealing temperature. A red shift of the Raman peak is detected following Sb implantation and this increases with RTA at 600 °C. A number of factors may contribute to this Si Raman peak shift, including stress, phonon confinement effects [7] and increased carrier concentration [8]. The broadening of the Si Raman peak and red-shift of the peak position is indicative of confinement effects resulting from partial amorphisation of the strained Si layer during ion implantation. Since translational symmetry breakdown is expected in the ion-implanted samples resulting in a relaxation of the momentum conservation rule, the Raman spectra were studied in terms of a phonon correlation length model. This confinement model, first developed by Richter [9] and Campbell and Fauchet [10] is modified slightly to model our Raman spectra following Sb ion-implantation. In a perfect crystalline semiconductor, the long-range

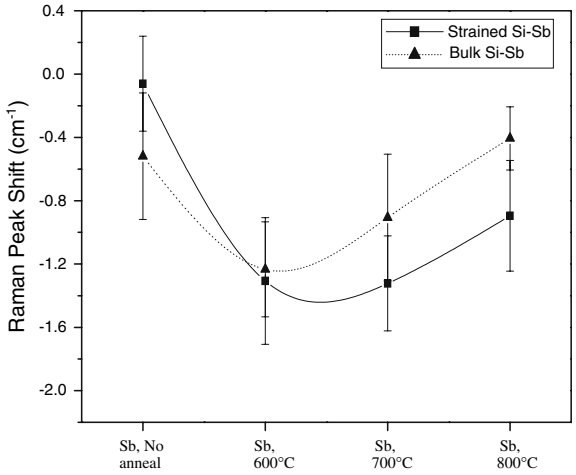

Fig. 5 Normalised peak shift of the Si–Si Raman mode in Sb-implanted Strained and Bulk Si substrates

periodicity of the lattice makes the correlation length of the normal-mode vibrations infinite, giving rise to the momentum selection rule, which limits Raman scattering to zone-centre ($q = 0$) optical phonon modes. The bulk, plane-wave-like phonon wavefunction cannot exist within a small crystallite. The spatial confinement, via the Heisenberg uncertainty principle, results in light scattering from a nominally zone-centre phonon whose wavevector has an uncertainty Δq and whose energy thus has an uncertainty $\Delta\omega$. Thus the phonon's spatial confinement results in a broadening of the Raman scattering features reflecting the uncertainty in its energy and a red shift of the Raman peak position occurs with increasing spatial confinement, as lower-energy bulk-like phonons are incorporated into the wavefunction describing the nominally zone-centre confined phonon. The model used by Macia et al. [7] to study silicon-on-insulator samples obtained by high dose oxygen ion implantation is adapted by introducing the parameter ω_0, which represents the stress-induced Raman line shift. Assuming a constant correlation length L in the scattering volume, the intensity of the first order Raman band of silicon is given by

$$I(\omega) \propto \int_0^{2\pi/a_0} \frac{|C(q)|^2 4\pi q^2 dq}{(\omega - \omega_0 - \omega(q))^2 + (\Gamma_0/2)^2} \quad (1)$$

where a_0 is the lattice constant of Si and Γ_0 is the Raman intrinsic line width of crystalline Si. The weight factor $C(q)$ for the scattering with wave vector q is given by

$$|C(q)|^2 \propto \exp\left(\frac{q^2 L^2}{8}\right) \quad (2)$$

$\omega\,(q)$ is the phonon dispersion relation, taken as

$$\omega(q) = \omega_p - 120\left(\frac{q}{q_0}\right)^2 \quad (3)$$

where ω_p is the wave number of the first order Raman band in the absence of disorder effects (520 cm^{-1}) and $q_0 = 2\pi/a_0$. The experimental data were fitted by varying the parameters ω_0 and L, so that the stress effect (contained in the parameter ω_0) can be decoupled from those due to residual damage (contained in the parameter L which gives an indication of the average distance between defects). The result of the fitting procedure is shown in Fig. 6. The phonon correlation length estimated from the theoretical fit of the spectrum is 30 Å. The intrinsic Si line width was chosen as 3.5 cm^{-1}, in agreement with our FWHM value obtained for bulk Si, and ω_0 was set to 5.3 to account for the shift in the Raman spectrum due to stress. A shift of –5.3 cm^{-1} implies a tensile stress of 1.33 GPa, which indicates that slight relaxation of the thin strained Si layer (measured stress of 1.41 GPa before implantation) has occurred during ion implantation. The small net red-shift of the Si Raman peak position of the strained Si sample following ion implantation, of the order of –0.1 cm^{-1} (Fig. 5) is accounted for by confinement effects.

This confinement model is no longer valid for the annealed samples due to the recovery of the lattice. However, a further increase in the red-shift of the Si Raman peak occurs following RTA at 600 °C. Due to the difficulty of extracting very small differences in the Raman Si peak position, the measurements were repeated several times and the error bars plotted in Fig. 5 represent a standard deviation from the average value. Although the error bars are not insignificant, a clear general trend emerges where the maximum Si peak shift is found in the range of 600–700 °C in both bulk and strained Si, and a small reduction in the red-shift is detected in samples annealed at 800 °C.

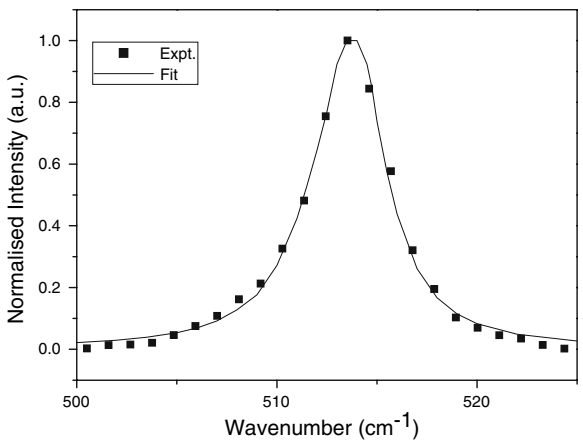

Fig. 6 Experimental points and theoretical (solid line) fit of the Raman spectrum of strained Si after Sb implantation

An early study on the dependence of the first-order Raman frequency of n-type Si as a function of carrier concentration found that the frequency of the Si peak decreases as the electron carrier concentration increases [8]. This effect can be explained by a lowering of the average energy of the free carriers due to the splitting of the X-point degeneracy of the conduction band, resulting in a smaller contribution to the free energy, which produces a softening of the lattice [8]. Measurements of the sheet carrier concentration of these samples recently published by us [11] have shown maximum values at 600–700 °C, before a reduction in carrier concentration at 800 °C. This result agrees with the measured shift in the Si Raman peak position following heat treatment. For annealed samples, the absolute values of the Raman peak shift are smaller in the case of bulk Si compared to strained Si. Again this is consistent with the interpretation that a carrier concentration effect is playing a role in the Raman peak shift as we have shown that 0.7% strain has doubled the amount of electrically active Sb compared to Sb implants in bulk Si [11]. Cerdeira and Cardona [8] developed a formula describing the Raman frequency shift as a function of carrier concentration, N. For n-type Si this is given by:

$$10^3\left(\frac{\Delta\omega}{\omega_p}\right) = -0.025X\left(1 + 0.02X^{2/3}\right) \quad (4)$$

where $X = 10^{-19}N$ and ω_p and $\Delta\omega$ are the wave number of the first order Raman band in the absence of strain or disorder effects and the Raman shift from this position, respectively. The carrier concentration calculated from the Raman shift using UV Raman will reflect the average carrier concentration over the probed volume to a depth of ~9 nm. The average carrier concentration of a Sb-implanted strained Si sample annealed at 700 °C measured using the differential Hall technique is 7.1×10^{20} cm^{-3} [11]. By way of example, from Eq. 4 this would imply a Raman peak shift of –1.24 cm^{-1}, and would therefore largely account for the measured peak shift of –1.32 cm^{-1} at 700 °C plotted in Fig. 5. However, at this stage of our investigations we would not rule out a further contribution to this peak shift due to a small change in strain following activation of dopants by heat treatment.

4 Conclusions

Sb is suggested as a possible alternative dopant to As for use in ultrashallow source-drain regions in future CMOS devices. A significant drop in resistivity is measured for Sb compared to As doping in strained Si. Micro-Raman spectroscopy has shown that the damage induced by low energy ion-implantation is mostly repaired by low thermal-budget heat treatment in the range of 600–800 °C. A correlation has been found between the frequency of the Si Raman peak and the electron carrier concentration.

Acknowledgements Science Foundation Ireland is gratefully acknowledged for funding this project under the Investigator Programme Grant. The authors would like to thank IQE Silicon Compounds Ltd. for providing the strained silicon substrates used in these experiments. We acknowledge ANKA, HASYLAB and the European Community for funding under Contract RII3-CT-2004_506009 (IA-SFS). We are grateful to R. Simon of ANKA for assistance in using the Topas beamline and T. Wroblewski and C. Paulmann for their help at HASYLAB beamline F-1.

References

1. S. Thompson, P. Packan, M. Bohr, Intel Technol. J. Q3'98
2. T. Alzanki, R. Gwilliam, N. Emerson, B.J. Sealy, Appl. Phys. Lett. **85**, 1979 (2004)
3. N.S. Bennett, A.J. Smith, C.S. Beer, L. O'Reilly, B. Colombeau, G.D. Dilliway, R. Harper, P.J. McNally, R. Gwilliam, N.E.B. Cowern, B.J. Sealy, Mater. Res. Soc. Symp. Proc. **912**, C2.3 (2006)
4. G.D.M. Dilliway, A.J. Smith, J.J. Hamilton, J. Benson, L. Xu, P.J. McNally, G. Cooke, H. Kheyrandish, N.E.B. Cowern, Proc. IIT NIM-B **237**, 131 (2005)
5. I. de Wolf, Semicond. Sci. Technol. **11**, 139 (1996)
6. B. Pichaud, M. Putero, N. Burle, phys. stat. sol. (a) **171**, 251 (1999)
7. J. Macía, E. Martín, A. Pérez-Rodríguez, J. Jiménez, J.R. Morante, B. Aspar, J. Margail, J. Appl. Phys. **82**, 3730 (1997)
8. F. Cerdeira, M. Cardona, Phys. Rev. B **5**, 1440 (1972)
9. H. Richter, Z.P. Wang, L. Ley, Solid State Commun. **39**, 625 (1981)
10. I.H. Campbell, P.M. Fauchet, Solid State Commun. **58**, 739 (1986)
11. N.S. Bennett, N.E.B. Cowern, A.J. Smith, R.M. Gwilliam, B.J. Sealy, L. O'Reilly P.J. McNally, G. Cooke, H. Kheyrandish, Appl, Phys. Lett. **89**, 182122 (2006)